

Fractal Investigation of Temporal Distribution of Simulated Phase Variables of a chaotic dynamic system

Salau T. A.O.¹ and Ajide O.O.²

Department of Mechanical Engineering, University of Ibadan, Nigeria

^{*}ooe.ajide@ui.edu.ng²; tao.salau@ui.edu.ng¹

*Corresponding Author

Abstract: This study investigated the temporal/near re-occurrence of simulated phase variables in chaotically responding nonlinear Duffing oscillator using fractal dimension when excited harmonically. The unsteady and steady phase variables were simulated from three different initial conditions by the constant step fourth order Runge-Kutta algorithms while the fractal characterization was achieved by the box-counted method. A total of 8,192 boxes arranged edge-to-edge on the time axis and with equivalent size of simulation time step were used to store the simulated phase results that are within 0.02 tolerance limit relative to specified standard. However, the fractal dimensions estimate were based on 14-different resolution scales. The results show temporal distribution of simulated phase variables that shared qualitative and quantitative similarities with Cantor set. The estimated fractal dimensions were between 0.0 to 0.58 and 0.0 to 0.65 for displacement and velocity component respectively. The distribution of the estimated fractal dimensions shows distinct peak values for the initial conditions. The addition of corresponding peak values of the estimated fractal box dimension from the displacement and velocity components are 1.10, 1.09 and 1.12 for the initial conditions of (-1, 0), (0, 0) and (1, 0). These estimates can be used to predict the fractal dimension of the corresponding Poincare section to within 14.9% maximum absolute error.

[Salau T. A.O. and Ajide O.O. **Fractal Investigation of Temporal Distribution of Simulated Phase Variables of a chaotic dynamic system.** *N Y Sci J* 2015;8(9):6-14]. (ISSN: 1554-0200). <http://www.sciencepub.net/newyork>. 2

Keywords: Chaotic system, Fractal, Temporal distribution, Cantor set and Duffing oscillator

1. Introduction

Researchers have found fractal to be an important concept in dynamics. It is interestingly becoming one of the main fundamentals in chaos theory and nonlinear dynamics. Although the theory of chaos and the concept of fractals evolved independently, studies have shown that they have penetrated each other's front and are highly interdependent. Exhaustive literature has shown fractal concept to be a resourceful tool for investigating interesting properties of chaotic dynamics. The main interesting properties of chaotic systems are nonperiodic and complex temporal behaviour, sensitive dependence on initial conditions, fractal structure and long term unpredictability (Aihara, 2002). Among these interesting dynamic properties, researchers' attentions and interests have shifted to the study of temporal and spatio-temporal dynamic behaviours (Brindley et al, 1994; Baier and sahle, 1997; Nakao, 1999; Cai, 2001; MacIntosh et al, 2013; Zamani et al, 2014). Temporal property in dynamics refers to all properties of a system that varies with time. Temporal system sometime shares certain properties with cantor set. A Cantor set has been described as closed, totally disconnected, and perfect subset of a closed interval. The significance of cantor set in describing temporal distribution dynamics is enormous. Extensive works have been done by researchers in this field on the characterization of temporal distribution in system

dynamics. Pathirana et al (2003) work was on estimating rainfall distributions at high temporal resolutions using a multifractal model. A multifractal model based on the scaling properties of temporal distribution of rainfall intensity was formulated to investigate the intensity distribution relationships in the available scaling regime. The findings obtained from the study have provided a clue to means of relating rainfall distributions at various temporal scales. In order to simulate and predict the air pollutant concentration data, Ho et al (2004) studied the temporal variations of PM₁₀ concentration in Taipei using fractal approach. A simple generalised cantor set with two rescaling parameters and measured parameters was employed to model multifractal spectra of PM₁₀ concentration time series. Although it was reported in the paper that it is difficult to conclude that PM₁₀ is governed by a single two-scale cantor set, the results obtained can be considered as a satisfactory model for temporal distribution of PM₁₀ concentrations. The authors' paper provides some insight on the temporal distribution of a dynamic system. Analysis of high impedance faults using fractal approaches has been carried out (Mamishev et al, 1996). The application of the concepts of fractal geometry in the analysis of high impedance faults was described in the authors' paper. The temporal behaviour of high impedance faults was examined using Root Mean Square (RMS). The paper showed that the temporal dynamics of power system currents

is usually of low dimensions with 1.0 to 2.0 fractal dimensions. The authors' paper has demonstrated the relevance of temporal dynamics in detection of impedance faults in power system. A temporal distribution of microseismicity using fractal technique was carried out by Latora et al (1998). The authors analysed a catalog of micro-earthquakes recorded by the four stations in the low eastern flank of Mt Etna during the period 1989-1994. The authors found that fractal clustering is very probably linked to the onset of the two eruptive phenomena that occurred in the same period. A chaotic perspective of rainfall dynamics at different scales has been examined (Sivakumar, 2001). The correlation dimensions for the four rainfall series implied the possible existence of a chaotic behaviour. The paper concluded that the presence of chaotic behaviour could provide interesting openings for a better understanding of the rainfall transformation process. In the same vein, a study which explored the invariance of properties manifested across scales and the determination of fractal cum multifractal behaviour observed in the temporal structure of rainfall using daily data has been carried out (Taouti, 2014). The paper adopted box-counting technique in order to determine the fractal dimension of daily rainfall data. The outcome of the study has given a deep insight to the temporal distribution of rainfall in a Mediterranean climate in northern Algeria. Telesca et al (2004) carried out an investigation of scaling properties in temporal patterns of seismic sequences by means of fractal techniques. The multifractal spectrum parameters derived from the analysis of the shape of the singularity spectrum has been used to measure the complexity of seismicity. Kozelov (2005) investigated the temporal dynamics of aurora by exploring available information about the spatial distribution of auroral luminosity in order to characterize the metric in "space of images". The author's article has indeed provided some understanding on the application of temporal chaos in television images. Enescu et al (2005) studied the temporal distribution of events in a paper that focused on Multifractal and chaotic analysis of Vrancea intermediate-depth earthquakes. In the first part of the work, multifractal characteristics of the temporal distribution of the earthquakes were analyzed. The outcome of the first part of the work showed two distinct scaling regimes. A clear non-homogeneous and multifractal pattern was found at small scales. At large scales, the temporal distribution of events showed a monofractal and close to random behaviour. The authors' paper has enriched one's understanding about the relevance of temporal distribution. The concept of temporal distribution was also applied in Gutiérrez et al (2006) paper. In the authors' paper, characterization of temporal precipitation distribution

using chaos game was carried out. The study showed that different climates exhibit characteristic patterns with different fractal exponents and entropies. The paper has indeed provided a useful application in climate classification and characterization of temporal precipitation aggregation patterns. One of the most seismically active areas in Italy was examined by (Telesca and Lovallo, 2008). The outcome of the study showed significant deviations from uniform power-law scaling in the seismic temporal fluctuations which were mostly linked with the occurrence of rather large earthquakes or seismic clusters. The evolution of the temporal multifractal scaling properties of the Chiayi earthquake in Taiwan has been investigated (Tang et al, 2012). The study revealed that variations in the fractal dimension of earthquake may be used as a precursor of a large earthquake.

Despite the immense efforts made so far on characterization of temporal distributions using fractal approach, literature is very sparse on the study of temporal distribution of simulated phase variables of a chaotic dynamic system. The identified research gap motivated this present study which examined the temporal distribution of simulated phase variables in a nonlinear harmonically excited Duffing oscillator using fractal dimension as a characterization tool.

2. Methodology

The dimensionless second order differential equation (1) abstracted the harmonically excited Duffing oscillator used in this study and was reported to have chaotic response under some drive parameters in Moon (1987), Dowell (1988) and Narayanan and Jayaraman (1989b).

$$\ddot{x} + \gamma \dot{x} - \frac{x}{2}(1-x^2) = P_o \sin(\omega t) \quad (1)$$

Equation (1) refers, x , \dot{x} and \ddot{x} represents respectively displacement, velocity and acceleration of the oscillator about a set datum over time (t). The drive parameters are damp coefficient (γ), excitation amplitude (P_o) and, excitation frequency (ω). Equation (1) can be simulated using fourth order Runge-Kutta algorithms only when it is represented as a pair of first order differential equivalent as in equations (2) and (3). The transformation procedure assumed (x_1, x_2) as displacement and velocity component.

$$\dot{x}_1 = x_2 = f_1 \quad (2)$$

$$\dot{x}_2 = P_o \sin(\omega t) - \gamma x_2 + \frac{x_1}{2} (1 - x_1^2) = f_2 \quad (3)$$

The present study utilized the equilibrium positions of the Duffing oscillator as initial conditions. In view of this and with reference to equations (2) and (3) the un-excited Duffing oscillator has three equilibrium positions which are $(x_1, x_2 \equiv -1, 0)$, $(x_1, x_2 \equiv 0, 0)$, and $(x_1, x_2 \equiv 1, 0)$. The corresponding Jacobian matrix is given by equation (4). Evaluation of this equation as a function of eigenvalue (λ) at $(x_1, x_2 \equiv 0, 0)$ yield the characteristic equation 5 and at $(x_1, x_2 \equiv -1, 0)$ or $(x_1, x_2 \equiv 1, 0)$ yield equation 6. The solutions to equations (5) and (6) are given by equation (7) and (8) respectively. Thus $(x_1, x_2 \equiv 0, 0)$ is an unstable saddle while $(x_1, x_2 \equiv -1, 0)$ and $(x_1, x_2 \equiv 1, 0)$ are stable focus.

$$\begin{bmatrix} \frac{\partial f_1}{\partial x_1} & \frac{\partial f_1}{\partial x_2} \\ \frac{\partial f_2}{\partial x_1} & \frac{\partial f_2}{\partial x_2} \end{bmatrix} \quad (4)$$

$$\lambda^2 + \gamma\lambda - \frac{1}{2} = 0 \quad (5)$$

$$\lambda^2 + \gamma\lambda + \frac{1}{2} = 0 \quad (6)$$

$$\lambda_{1,2} = \frac{-\gamma \pm \sqrt{(\gamma^2 + 2)}}{2} \quad (7)$$

$$\lambda_{1,2} = \frac{-\gamma \pm \sqrt{(\gamma^2 - 2)}}{2} \quad (8)$$

2.1 Fourth-order Runge-Kutta algorithms

The popular fourth-order Runge-Kutta algorithms scheme is given by equations (9) to (13), in which y_{1+i} and y_i represent any of the phase variables being simulated at iteration time nodes $1+i$

and i respectively. The simulation of the displacement and velocity components is done simultaneously at constant time step (h) taking respectively $f \leftarrow f_1$ and $f \leftarrow f_2$ for displacement and velocity component.

$$y_{i+1} = y_i + \frac{h}{6} \{ K_1 + 2(K_2 + K_3) + K_4 \} \quad (9)$$

$$K_1 = f(t_i, y_i) \quad (10)$$

$$K_2 = f(t_i + \frac{h}{2}, y_i + \frac{K_1 h}{2}) \quad (11)$$

$$K_3 = f(t_i + \frac{h}{2}, y_i + \frac{K_2 h}{2}) \quad (12)$$

$$K_4 = f(t_i + h, y_i + K_3 h) \quad (13)$$

2.2 Simulation Parameters

The present study used $\gamma = 0.168$, $P_o = 0.21$, and $\omega = 1.0$ because Dowell (1988) reported chaotic response of the Duffing oscillator for these parameters combination. The simulation of the transient and steady solutions of equations (2) and (3) with the fourth order Runge-Kutta algorithms was driven at constant time step ($h = \Delta t = T_p / 100$) in which $T_p = 2\pi/\omega$. The transient and steady simulation period spanned the first twenty ($20T_p$) and the next ($140T_p$) consecutive excitation periods respectively. The reference phase variables (5000) were selected consecutively from the steady solutions in the first fifty ($50T_p$) simulation periods. The temporal distribution of the remaining steady solutions that are within 0.02 tolerance relative to selected specified reference value were noted appropriately in 8192 lined-up boxes of size (h). Thereafter these were analyzed for their corresponding estimated box dimension using the box-counted method and utilizing the selected reference phase variables one after the other. The procedure is very similar to that used by Salau and Oke (2013) for the fractals analysis of English alphabets in a doctoral thesis.

2.3 Box-counted Method

The power law relationship is expected between the variation of the scale of observations (X) and the corresponding box-counted (Y) when using the box-counting method for estimating the fractal box dimension (D), hence the proportional equation (14). A straight line equation (15) with intercept $\log(\kappa)$ and slope (D) is obtained when a constant of proportionality (κ) is introduced and logarithm of both sides of equation (14) taking. The slope of the line of best fit to fourteen (14) observed data points is

accepted as estimate of fractal box dimension for the present study.

$$Y \propto X^D \quad (14)$$

$$\log(Y) = \log(\kappa) + D \log(X) \quad (15)$$

3. Results and Discussion

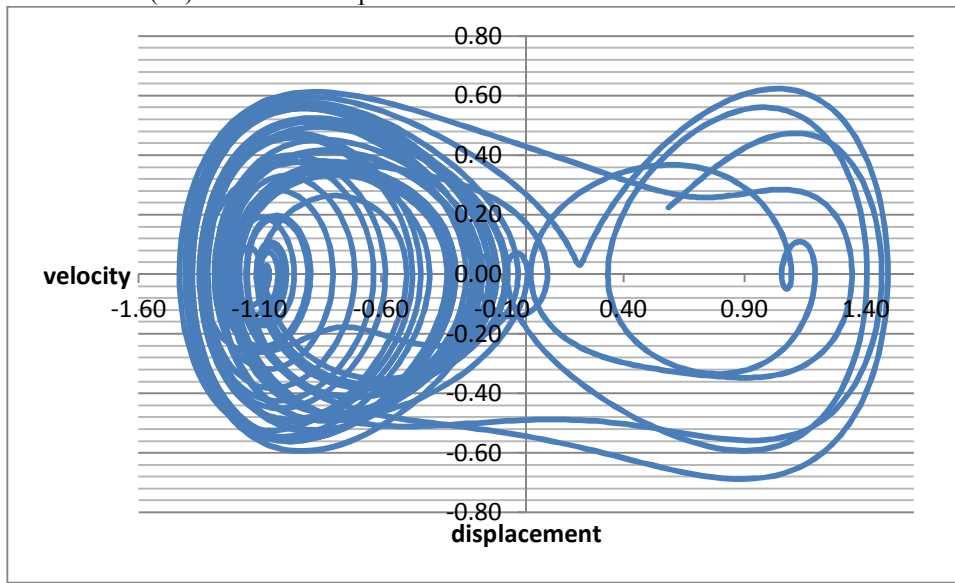


Figure 1: Phase plots of steady simulation results in the time interval ($20T_p \leq \text{Time} < 50T_p$) when the simulation initial conditions is (-1, 0).

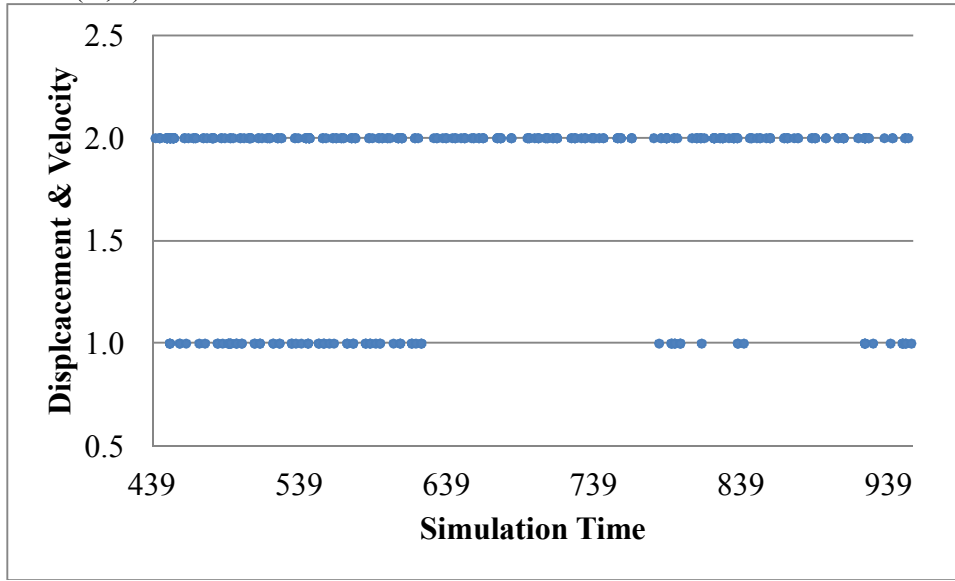


Figure 2: Temporal distribution/re-occurrence at 0.02 tolerance of displacement (bottom, 0.58612) and velocity (top, 0.22397) components in the steady simulation time interval ($70T_p \leq \text{Time} < 152T_p$) when the simulation initial conditions is (-1, 0).

The phase plots shown in figure 1 was simulated with $\gamma = 0.168$, $P_o = 0.21$, and $\omega = 1.0$ from initial conditions $(-1, 0)$ and have dynamic interpretation of chaotic response of the Duffing oscillator. This agreed with the report of Dowell (1988) for the combination of these drives parameters and thus validated the FORTRAN95 language simulation codes developed for the present study.

The displacement (bottom) and velocity (top) distribution/re-occurrence at 0.02 tolerance shown in

figure 2 is very similar in visual appearance to Cantor dust (with a fractal dimension of 0.631) discussed in Barnsley (1993) and Edward (1996). Quantitatively the box dimensions are 0.454 and 0.615 respectively for displacement and velocity components, see table 1 and figure 3. The box dimensions (D) are equivalent to the slope of line of best fit to the log-log plots of scale and the counted number of filled boxes for the displacement and velocity components.

Table 1: Variation of number of filled boxes with increasing resolution for displacement (0.58612) and velocity (0.22397) components in the steady simulation time interval ($70T_p \leq Time < 152T_p$) when the simulation initial conditions is $(-1, 0)$.

Resolution (Scale=X)	Number of filled Boxes (Y)		Natural logarithms of Scale and number of filled boxes		
	Displacement	Velocity	Scale	Displacement	Velocity
1	1	1	0.00	0.00	0.00
2	2	2	0.69	0.69	0.69
4	4	4	1.39	1.39	1.39
8	6	8	2.08	1.79	2.08
16	10	16	2.77	2.30	2.77
32	18	32	3.47	2.89	3.47
64	29	61	4.16	3.37	4.11
128	42	94	4.85	3.74	4.54
256	46	122	5.55	3.83	4.80
512	47	133	6.24	3.85	4.89
1024	48	144	6.93	3.87	4.97
2048	52	169	7.62	3.95	5.13
4096	60	211	8.32	4.09	5.35
8192	82	297	9.01	4.41	5.69

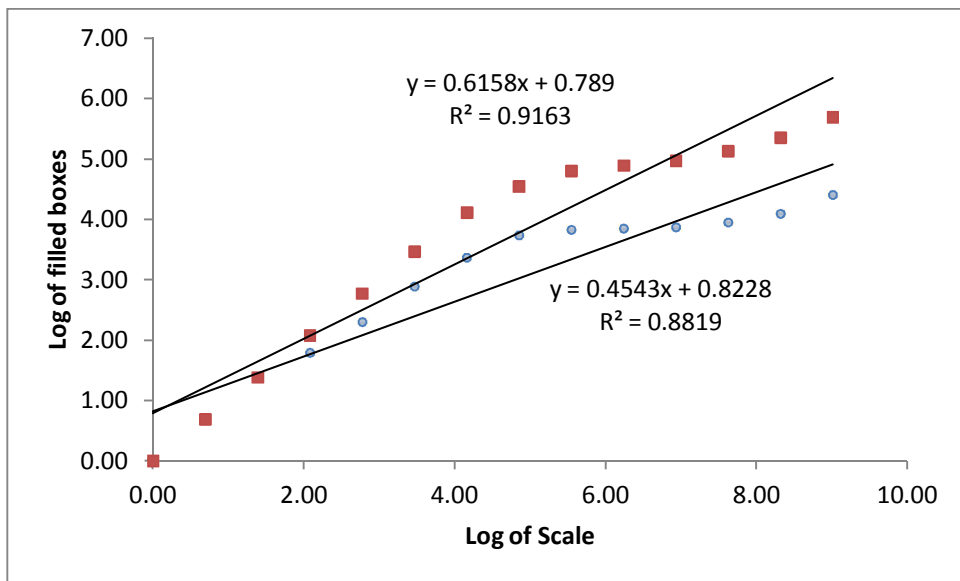


Figure 3: Log-log plots of resolution (scale) and the counted number of filled boxes.

Table 2: Estimated fractal box dimensions for sample of twenty out of 5001 investigated points when simulation initial conditions is $(-1, 0)$.

Phase Point		Number of filled boxes out of 8192		Fractal box dimension (D) of temporal distribution of filled boxes	
Displacement	Velocity	Displacement	Velocity	Displacement	Velocity
0.58612	0.22397	82	297	0.454	0.616
0.60051	0.23404	91	293	0.477	0.613
0.61555	0.24480	89	301	0.468	0.614
0.63128	0.25619	99	326	0.485	0.620
0.64775	0.26817	96	330	0.481	0.620
0.66499	0.28069	92	334	0.478	0.624
0.68303	0.29368	92	324	0.475	0.617
0.70191	0.30708	80	318	0.473	0.615
0.72163	0.32078	98	348	0.488	0.618
0.74222	0.33471	108	344	0.498	0.615
0.76369	0.34876	98	325	0.488	0.606
0.78605	0.36282	94	286	0.488	0.592
0.80928	0.37675	97	252	0.489	0.576
0.83339	0.39043	101	230	0.492	0.567
0.85834	0.40369	102	205	0.493	0.550
0.88410	0.41638	112	223	0.504	0.556
0.91065	0.42832	114	206	0.507	0.548
0.93791	0.43932	122	202	0.517	0.546
0.96583	0.44919	125	218	0.513	0.550
0.99433	0.45773	121	238	0.516	0.558

Table 3 refers. The numbers of filled boxes out of 8192 maximum possible for the displacement component remain consistently lower than that of the velocity component of the phase points studied. For instance for the phase point $(0.99433, 0.45773)$ the corresponding number of filled boxes is $(121, 238)$. However despite the fact that the filled boxes for the velocity component almost double that of the displacement counterpart there is only absolute difference of 0.042 in the estimated fractal box dimensions $(0.516, 0.558)$. This is re-affirmation of the fact that the estimated fractal box dimension is highly dependent on the temporal distribution and not actual number of filled boxes. Based on a total of 5001 studied displacement value points, the number of filled

boxes lies in the limits 8-242 and the estimated fractal box dimension lies between 0.181-0.575. The corresponding results for the velocity component is 10-390 limit values for the number of filled boxes while the estimated fractal box dimension lies between 0.204-0.648.

The results reported in figures 1 to 3 and tables 1 to 3 were similarly obtained for the studied initial conditions $(0, 0)$ and $(1, 0)$, but the results not presented here only to save space. However the normalized distribution of the estimated fractal box dimensions in 100-equal intervals between minimum and maximum estimated box dimension are presented in figures 4 to 6 for the respective studied initial conditions $(-1, 0)$, $(0, 0)$ and $(1, 0)$.

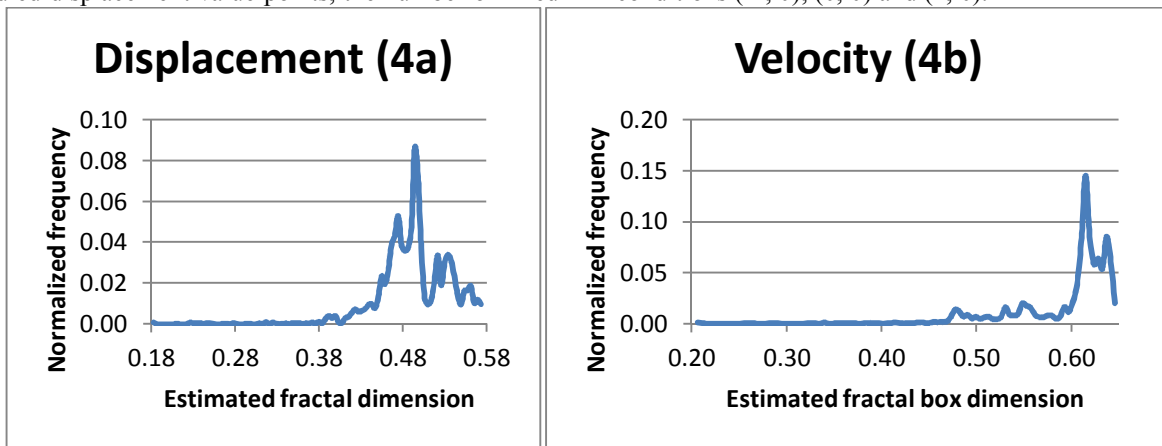


Figure 4: Normalized distribution of the 5001 estimated fractal box dimension for the initial conditions $(-1, 0)$.

The distributions of estimated fractal dimensions shown in figure 4 have peak values of 0.49 and 0.61 for respective displacement and velocity components.

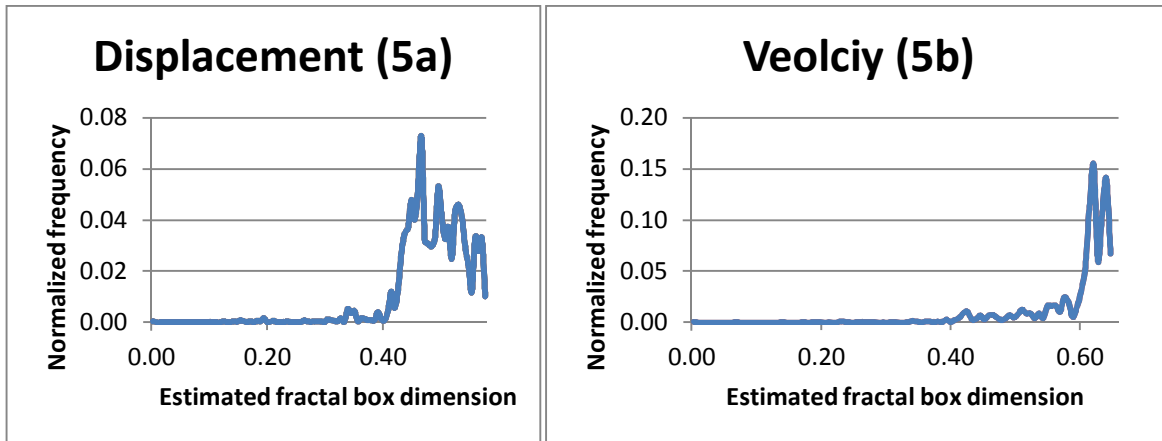


Figure 5: Normalized distribution of the 5001 estimated fractal box dimension for the initial conditions (0, 0).

The distributions of estimated fractal dimensions shown in figure 5 have zero value lower limits in common and peak values of 0.47 and 0.62 for the respective displacement and velocity components. The

observation is expected because the number of filled boxes is between 0-241 and 0-382 for the displacement and velocity components respectively.

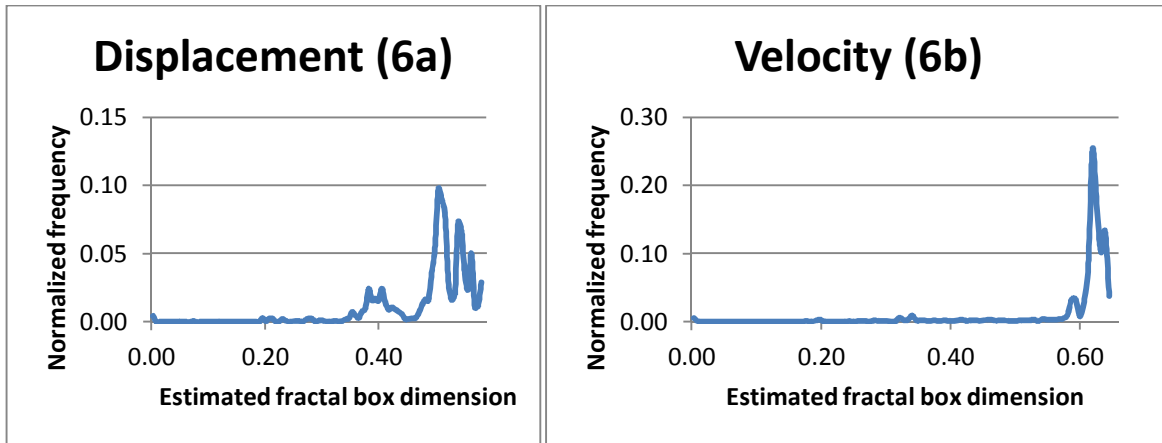


Figure 6: Normalized distribution of the 5001 estimated fractal box dimension for the initial conditions (1, 0).

Though the initial conditions (-1, 0) and (1, 0) are stable focus the corresponding estimated fractal box dimension distributions of figures 4 and 6 lacked resemblance. Furthermore, as observed in figure 5, the distributions of estimated fractal dimensions shown in figure 6 have zero value lower limits in common and peak values of 0.50 and 0.62 for the respective displacement and velocity components. The observation is expected because the number of filled

boxes is between 0-202 and 0-372 for the displacement and velocity components respectively.

Figures 4 to 6 refer. All the distributions skewed toward higher estimated fractal box dimension value. The addition of peak values of the estimated fractal box dimension from the displacement and velocity components are 1.10, 1.09 and 1.12 for the corresponding initial conditions of (-1, 0), (0, 0) and (1, 0). The maximum percentage absolute difference between each of these values and the optimum fractal

disk dimension (1.2815) of the Poincare section for the same Duffing oscillator drive parameters reported by Salau and Ajide (2012) is 14.9%. The large percentage difference can be accounted by differences in computation methods and simulation time steps. Salau and Ajide (2012) used optimum disk counted method to analyze periodically reported phase variables over a very large number of iteration periods and shorter iteration step. However the iteration time step is higher for the current method and data used were collected from the relatively shorter time history of simulated phase variables.

4. Conclusions

This study has demonstrated the existence of qualitative and quantitative resemblance between the temporal distribution of a dynamic system phase variables and the Cantor set. The displacement temporal distribution compare visually well with Cantor set while the velocity counterpart compare very well with Cantor set in quantitative term. Moreover this study shows that the sum of the peak dimension values from the fractal analysis of the temporal distribution of phase variables can be used to predict the fractal dimension of the corresponding Poincare section to within 14.9% maximum absolute error.

References

1. Baier G. and Sahle S. (1997), Spatio-Temporal patterns with hyperchaotic dynamics in diffusively coupled biochemical oscillator. *Discrete Dynamics in Nature and Society*, Vol.1, pp.161-167.
2. Barnsley, M. F. (1993), *Fractals Everywhere*, 2nd Ed. Academic Press, New York, 6-111.
3. Brindley J., Kaneko K. and Kapitaniak T.(1994), Spatio-Temporal chaos in closed and open systems. *Chaos, Solitons & Fractals*, Vol.4, No.7, pp.1193-1209.
4. Cai D., McLaughlin D.W. and Shatah J.(2001), Spatiotemporal chaos in spatially extended system, *Mathematics and Computers in Simulation*, Vol.55 , pp.329-340.
5. Dowell E.H. (1988), Chaotic oscillations in mechanical systems, *Computational Mechanics*, Vol.3, pp.199-216.
6. Edward R. S. (1996), *Invitation to Dynamical Systems*, Prentice Hall, Inc. A Simon & Schuster Company, Upper Saddle River, New Jersey 07458, 231-316.
7. Enescu B., Ito K., Radulian M., Popescu E. and Bazacliu O.(2005), Multifractal and chaotic analysis of Vrancea (Romania). *Intermediate-depth Earthquakes: Investigation of the temporal distribution of events. Pure and Applied Geophysics*, Vol.162, pp.249-271.
8. Francis C.M. (1987), *Chaotic vibrations-An Introduction for Applied Scientists and Engineers*, John Wiley & Sons, New York, ISBN 0-471-85685-1.
9. Gutiérrez J.M., Galvan A., Cofino A.S. and Primo C. (2006), Chaos game characterization of temporal precipitation variability: Application to regionalization. *Fractals: Complex geometry, patterns and scaling in nature and society*, Vol.14, No.2.
10. Ho D., Juang L., Liao Y., Wang C., Lee C., Itsu T., Yang S. and Yu C. (2004), The temporal variations of PM₁₀ concentration in Taipei: a fractal approach. *Aerosol and Air Quality Research*, Vol.4, No.1, pp.38-55.
11. Kozelov B.V. (2005), Search of temporal chaos in TV images of aurora. *International Journal of Geomagnetism and Aeronomy*, Vol.5, pp.1-5.
12. Latora V., Rapisarda A. and Vinciguerra S. (1998), A fractal approach to the temporal distribution of microseismicity at the low eastern flank of Mt Etna during 1989-1994. *Physics of the Earth and Planetary Interiors*, Vol.109, pp.115-127.
13. MacIntosh A.J.J, Pelletier L., Chiaradia A., Kato A. and Ropert-Coudert V. (2013), Temporal fractals in seabird foraging behaviours: diving through scales of time. *Scientific reports*, Vol.3, Article number 1884.
14. Mamishev A.V., Rusell B.D. and Benner C.L. (1996), Analysis of high impedance faults using fractal techniques. *IEEE transactions on power systems*, Vol.11, No.1, pp.435-440.
15. Nakao H. (1999), Anomalous spatio-temporal chaos in a two-dimensional system of nonlocally coupled oscillators. *Chaos*, American Institute of Physics, Vol.9, No.4, pp.902-909.
16. Narayanan S. and Jayaraman K. (1989), Control of Chaotic oscillations by vibration absorber. *ASME Design Technical Conference, 12th Biennial Conference on Mechanical Vibration and Noise*. DE 18.5, 391-394.
17. Salau T.A.O. and Oke S.A. (2013): An analysis on the application of rescale range and fractals in the characterization of English alphabets in a Doctoral Thesis, *The International Scientific Journal of Management Information Systems*, Vol. 8, No.1, 8-19.
18. Salau, T.A.O. and Ajide, O.O., (2012): Comparative Analysis of Numerically Computed Chaos Diagrams in Duffing Oscillator, *Journal of Mechanical Engineering and Automation (JMEA)*, Vol.2, No.4, pp.53-57.

19. Sivakumar B. (2001), Rainfall dynamics at different temporal scales: A chaotic perspective hydrology and Earth System Sciences, Vol.5, No.4, pp.645-651.
20. Tang Y., Chang Y., Liou T, Chen C. and Wu Y. (2012), Evolution of the multifractal scaling properties of the Chiayi earthquake ($M_L=6.4$), Taiwan. Tectonophysics, Vol.546-547, pp.1-9.
21. Taouti M.B.(2014), Fractal and multifractal analysis of the temporal structure of daily rainfall in a Mediterranean climate in northern Nigeria. Journal of Mediterranean Meteorology and climatology, Vol.11, pp.3-12.
22. Telesca L. and Lovallo M.(2008), investigating non-uniform scaling behaviour in temporal fluctuations of seismicity. Natural Hazards and Earth System Sciences, Vol.8, pp.973-976.
23. Telesca L., Lapenna V. and Macchiato M. (2004), Mono and multifractal investigation of scaling properties in temporal patterns of seismic sequences. Chaos, Solitons and Fractals, Vol.19, pp.1-15.
24. Zamani A., Azar A.K. and Safavi A. (2014), wavelet-based multifractal analysis of earthquakes temporal distribution in mammoth mountain volcano, monocounty eastern California. Acta Geophysica, Vol.62, Issue 3, pp.585-607.

8/31/2015